

Article

LCL Trap Filter Analysis with a PFC Isolated Ćuk Converter Using SiC MOSFET for DCM

Erdal Şehirli

Division Power Electronics, Silicon Austria Labs GmbH, Sandgasse 34, 8010 Graz, Austria; erdal.sehirli@silicon-austria.com

Abstract: The main contribution of the paper concerns the use of an LCL trap filter with a PFC isolated Ćuk converter. Further, SiC MOSFET is used with a PFC isolated Ćuk converter designed for 50 W with 42 kHz in DCM. A small-signal model of the converter is cascaded with the filter model to investigate the effect of the filter on the whole system. Moreover, large-signal and small-signal models of the converter are compared to investigate the requirement of the small-signal analysis. In addition, an LTspice simulation using SiC MOSFET of the system is conducted and the results are compared by the applications for both LC and LCL trap filters with respect to different loading conditions. Further, the LCL trap filter is compared with the LC filter regarding the PF, THD, and efficiency. Controller design considering the filter is also presented. In addition, the converter is operated and compared using linear and nonlinear loads for each filter. Parametric variation in the filter components is investigated. As a result of the simulation and applications, the THD of the grid current is 4.83% and the PF is 0.998, meeting the standards, and the overall efficiency of the system is 85% with the LCL trap filter. It can be concluded that the presented filter provides better results than the LC filter.

Keywords: LCL trap filter; isolated Ćuk; PFC; SiC; modeling; THD



Citation: Şehirli, E. LCL Trap Filter Analysis with a PFC Isolated Ćuk Converter Using SiC MOSFET for DCM. *Energies* **2024**, *17*, 758. <https://doi.org/10.3390/en17030758>

Academic Editors: Elena Breaz, Yigeng Huangfu, Shengrong Zhuo, Tianhong Wang and Wenshuai Bai

Received: 20 November 2023

Revised: 5 January 2024

Accepted: 12 January 2024

Published: 5 February 2024



Copyright: © 2024 by the author. Licensee MDPI, Basel, Switzerland. This article is an open access article distributed under the terms and conditions of the Creative Commons Attribution (CC BY) license (<https://creativecommons.org/licenses/by/4.0/>).

1. Introduction

A key concept in power electronics is the use of an input or electro-magnetic interference (EMI) filter. In order to reduce the high-frequency noises of the power switch in any kind of power converter, a filter has to be used with the connection of the power converter to the source. The source can be direct current or alternating current. The filter requirement is not just for the input side, but for the output side of the converter between loads as well. There are two main kinds of filter: active and passive. The application of an active filter is more complex than that of a passive filter. Therefore, the implementation of a passive filter does not involve much complexity. In addition, there are a wide variety of passive filters in use with the power converter. One of the most advanced filter types is LCL-type filters. However, the use of the LCL filter, particularly the LCL trap filter with the PFC converter type, is not presented in the literature. In addition, the need for galvanic isolation in the converter is gaining attention especially for battery charging application circuits. This isolation can be achieved by a high-frequency transformer or coupled inductance. A promising topology is the isolated Ćuk converter. Due to the presence of an inductor at both the input and output sides of the converter, the filter requirements are lower. Therefore, in the present paper, the isolated Ćuk converter has been selected as a converter.

A review of the relevant studies in the literature on the topic revealed the following. Ref. [1] introduces isolated Ćuk converter topology. The fundamental design of the converter is given in [2]. The converter is proposed as an LED driver in [3]. Ref. [4] gives a detailed modeling strategy for large- and small-signal models for DC–DC converters. Large signal average modeling is proposed using a neural network in [5]. Ref. [6] proposes a graph representation to model the converter for CCM and DCM operation for

using machine learning. A reduced order method to analyze the DCM buck converter is presented in [7]. Ref. [8] presents a new modeling strategy called the sigmoid function for power converters. Ref. [9] realizes the small-signal modeling of a two-phase boost converter having a coupled inductor for DCM. Modeling of the isolated Ćuk converter is given for DCM mode operation in [10,11]. Ref. [12] presents the small-signal modeling of an interleaved boost converter. Modeling of a fractional Zeta converter is derived in [13]. Ref. [14] describes the modeling of a boost converter with different software packages. The design and optimization of an LCL trap filter are given in [15]. Ref. [16] uses an LCL trap filter with an isolated Ćuk converter for DC source connection. The filter is used for the inverters as in [17]. Ref. [18] presents an annealing simplex method to select the inductance value in an LCL filter. Ref. [19] uses an LCL trap filter for two level converters with grid connection. The design for an LCL trap filter for AC–DC converters by using SiC MOSFET through simulations is shown in [20]. In order to reduce current harmonics under weak grid conditions of the converter, different trap filter structures are presented in [21]. Ref. [22] presents a new asymmetric LCL filter having an LC trap structure for grid-tied three-phase inverter applications.

Herein, the modeling and analysis of the LCL trap filter are carried out. Moreover, the filter effect on the isolated Ćuk converter using SiC MOSFET is investigated by a linear control methodology. The converter is operated in DCM with 42 kHz for 50 W power using linear and nonlinear loads with the LCL trap and LC filters. Furthermore, large-signal and small-signal models of the converter are derived and compared to examine the requirements of the small-signal analysis. Moreover, LTspice simulation is carried out using SiC MOSFET to compare results obtained by the applications. In addition, the results of LCL trap filter application and simulation are compared with the LC filter results and the standard. Further, parametric variation in the filter components is investigated. In conclusion, the LCL trap filter with the converter provides a 0.998 PF and 4.83% THD. These results are better than those of the LC filter and after comparison they meet the standards.

The structure of the paper is as follows. In Section 2, the LCL trap filter is introduced, its design methodology is given, and its transfer function is derived. In Section 3, the PFC isolated Ćuk converter is described, its design equations are given, and large- and small-signal models are derived with and without integrating the input filter. In Section 4, an open-loop LTspice simulation using L and LCL trap filters is given and closed-loop control application and measurements and comparison are presented. In Section 5, the findings are discussed and, in Section 6, the conclusion is given.

2. LCL Trap Filter

In the last two decades, the use of the LCL filter has gained much attention. The trap-type LCL filter is also an LCL-type filter but it includes a series inductor and capacitor in the middle of the filter as shown in Figure 1 as in [15,16]. However, the use of a trap filter with a single-phase PFC converter has not been described in the literature.

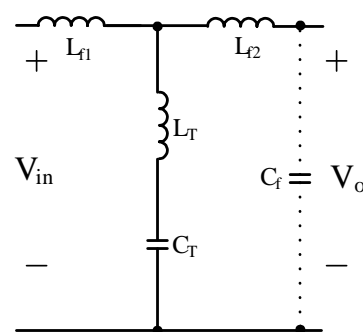


Figure 1. LCL trap filter.

The filter can be designed using (1)–(4) as in [15,16,23].

$$C_{f\max} = \frac{I_{pk}}{\omega_L V_{pk}} \tan \theta = \frac{\frac{P_0 \sqrt{2}}{V_s} \tan \theta}{\omega_L V_{pk}} = \frac{\frac{50 \sqrt{2}}{100} \tan 1}{376.8 \times \sqrt{2} \times 100} = 231.62 \text{ nF}, C_{f\max} \gg C_f \quad (1)$$

$$\omega_{res} = \sqrt{\frac{L_{f1} + L_{f2}}{C_T(L_{f1}L_{f2} + L_T L_{f2} + L_T L_{f1})}} \quad (2)$$

$$f_T = \frac{1}{2\pi \sqrt{L_T C_T}}, \quad f_T = f_s, \quad C_f = C_T, \quad (3)$$

$$10f_g < f_{res} < 0.5f_t \quad (4)$$

The filter transfer function can be derived in (5) as in [16].

$$T(s) = \frac{V_o}{V_{in}} = \frac{s^2 L_T C_T + 1}{\left(s^4 (L_{f2} C_f C_T L_T + L_{f2} C_f C_T L_{f1} + C_f C_T L_{f1} L_T) \right.} \quad (5)$$

$$\left. s^2 \left(C_f L_{f2} + C_T L_T + C_T L_{f1} + C_f L_{f1} \right) + 1 \right)$$

Related to the transfer function in (5), frequency domain analysis of the filter can be achieved by the Bode and root locus graphs in Figure 2. From the figure, it is seen that the filter has 4 poles and 2 zeros.

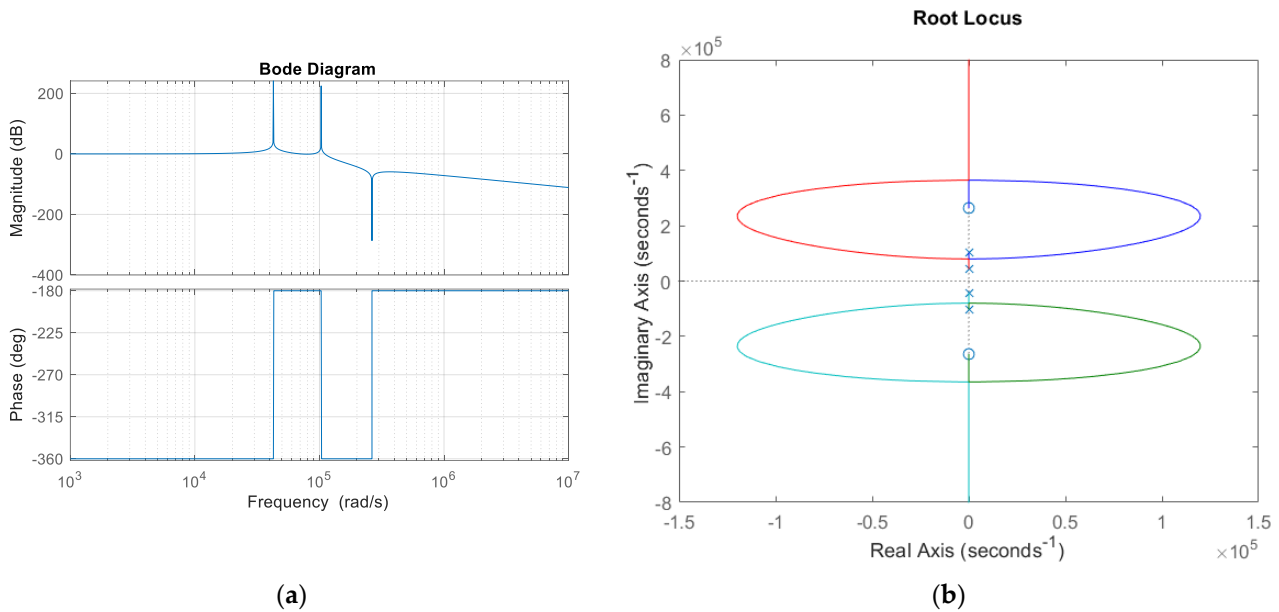


Figure 2. LCL trap filter (a) Bode; (b) root locus.

For observing the effect of the filter on the converter in terms of the control, the derived transfer function should be cascaded with the converter transfer function.

3. PFC Isolated Ćuk Converter

The structure of the converter with the filter is given in Figure 3. It is seen that the converter has a transformer and two inductors and capacitors and it is connected to the grid via a diode bridge and filter. The transformer is a high-frequency transformer and provides galvanic isolation.

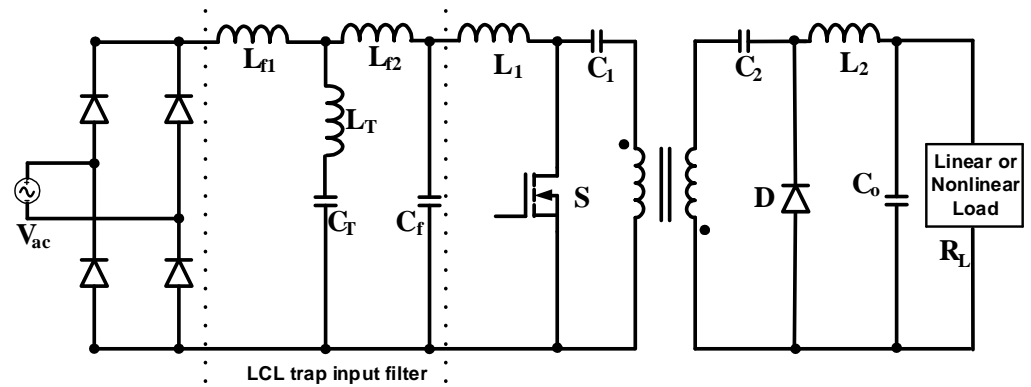


Figure 3. PFC isolated Ćuk converter with an LCL trap filter.

Converter parameters can be selected using (6)–(11) as in [2,10,16]. In the equations, d is the duty cycle, n is the turns ratio, V_{in} is the input voltage, V_o is the output voltage, L_1 and L_2 are the inductances, C_1 and C_2 are the intermediate capacitors, C_o is the output capacitor, and R_L is the load.

$$V_o = \frac{nV_{in}d}{(1-d)} \Rightarrow d = \frac{\frac{V_o}{n}}{V_{in} + \frac{V_o}{n}} = \frac{25 \times 5}{140 + 25 \times 5} = 0.47 \tag{6}$$

$$L_1 = \frac{R_L(1-d)^2}{2df_s n^2} = \frac{12.5(1-0.47)^2}{2 \times 0.47 \times 42000 \times 0.2^2} = 2.2\text{mH}, \tag{7}$$

$$L_2 = \frac{R_L(1-d)}{2f_s} = \frac{12.5(1-0.47)}{2 \times 42000} = 78.86\mu\text{H} \tag{8}$$

$$C_1 = \frac{V_{in}n^2d^2}{(1-d)\Delta V_{C1}f_s R_L} = \frac{140 \times 0.2^2 \times 0.47^2}{(1-0.47)12 \times 42000 \times 12.5} = 370\text{nF} \tag{9}$$

$$C_2 = \frac{V_o d}{\Delta V_{C2}f_s R_L} = \frac{25 \times 0.47}{24 \times 42000 \times 12.5} = 933\text{nF} \tag{10}$$

$$C_o \geq \frac{V_o(1-d)}{8L_2\Delta V_{C0}f_s^2} = \frac{25(1-0.47)}{8 \times 654 \times 10^{-6} \times 10 \times 42000^2} = 144\text{nF} \tag{11}$$

A mathematical model of the converter can be derived using the Kirchhoff voltage and current laws regarding switch on and off conditions. Because of the DCM operation, the converter has three different equivalent circuits as in [10]. The equivalent circuits are given in Figure 4 as in [10]. While deriving the model of the converter, it is assumed that the high-frequency transformer has ideal characteristics. Moreover, passive components are regarded as ideal, and the voltage drop in the switch is neglected.

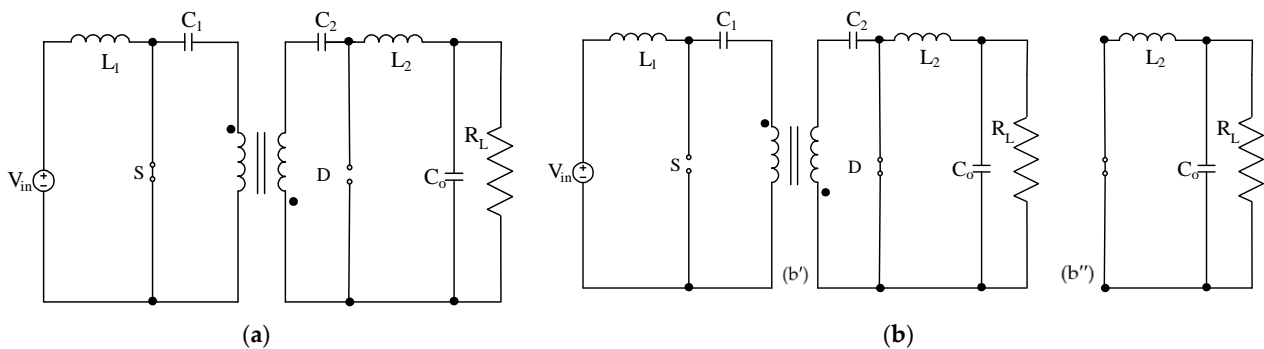


Figure 4. Equivalent circuit of the converter (a) switch on; (b) switch off. (b') switch off interval 1, (b'') switch off interval 2.

In the modeling strategy, time ratios of each interval regarding the input side inductor current are shown in Figure 5. It is seen that there are three different operation durations; these durations are identified as d duty cycle, δ , and $1-d-\delta$, matching the equivalent circuit in Figure 4 as in [24].

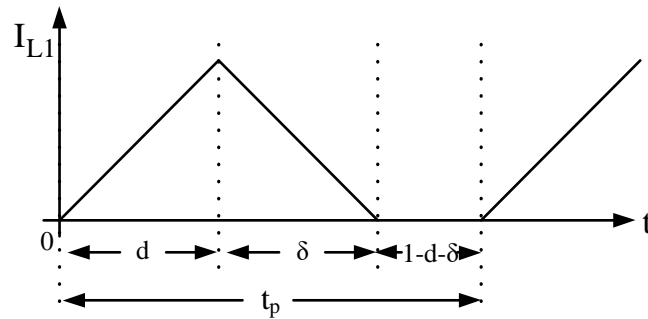


Figure 5. DCM mode operation intervals regarding inductor current.

Regarding Figure 5, the model for DCM of the converter can be derived using (12) as in [10,24].

$$A = dA_1 + \delta A_2 + (1 - \delta - d)A_3, B = dB_1 + \delta B_2 + (1 - \delta - d)B_3 \tag{12}$$

After applying (12) to each equivalent circuit, a mathematical model in state-space form is obtained in (13) as in [10].

$$\begin{bmatrix} \dot{i}_{L1} \\ \dot{V}_{C1} \\ \dot{i}_{L2} \\ \dot{V}_{C2} \\ \dot{V}_0 \end{bmatrix} = \begin{bmatrix} 0 & \frac{-\delta}{L_1} & 0 & \frac{-a\delta}{L_1} & 0 \\ \frac{\delta}{C_1} & 0 & \frac{-da}{C_1} & 0 & 0 \\ 0 & \frac{d}{aL_2} & 0 & \frac{d}{L_2} & \frac{-1}{L_2} \\ \frac{a\delta}{C_2} & 0 & \frac{C_1 d}{C_2} & 0 & 0 \\ 0 & 0 & \frac{-1}{RC_0} & 0 & \frac{-1}{RC_0} \end{bmatrix} \begin{bmatrix} i_{L1} \\ V_{C1} \\ i_{L2} \\ V_{C2} \\ V_0 \end{bmatrix} + \begin{bmatrix} \frac{d+\delta}{L_1} \\ 0 \\ 0 \\ 0 \\ 0 \end{bmatrix} V_{in} \tag{13}$$

The model given in (13) is built in Simulink 9.1 in Figure 6; this model can be called a large-signal model.

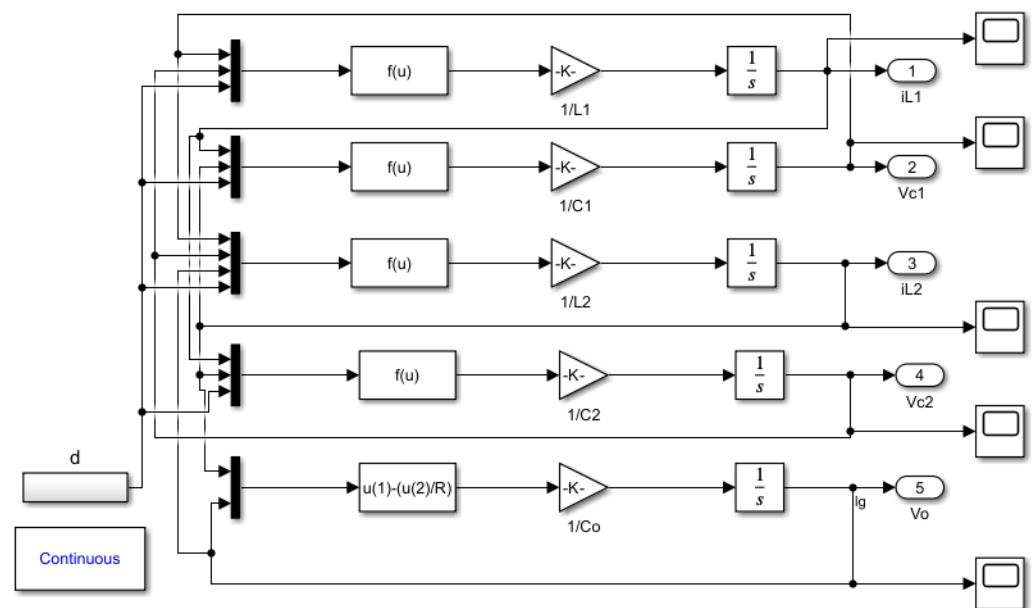


Figure 6. Large-signal model of the converter in DCM.

Due to the power switch, the model in (13) has nonlinear characteristics. To achieve linearization, a small-signal approach can be used. By using (14) as in [10,25], a control to output a small-signal transfer function can be derived in (15), as in [10,25]. While deriving the transfer function, steady-state values of the i_{L1} , i_{L2} , V_{C1} , and V_{C2} parameters should be replaced regarding V_{in} . In the equation, $k = \delta/d$ [10].

$$\dot{\tilde{x}} = (dA_1 + \delta A_2 + (1 - kd - d)A_3)\tilde{x} + [(A_1 + kA_2 - (k + 1)A_3)\bar{x} + (B_1 + kB_2 - (k + 1)B_3)u] \quad (14)$$

$$T(s) = \frac{\tilde{V}_0}{\tilde{d}} = \frac{s^3 \frac{(V_{in} - \frac{V_{in}d}{d-1})}{C_0 L_2 a} + s^2 \left(\frac{d \left(\frac{V_{in}kd^2}{R(d-1)^2} - \frac{dV_{in}}{Ra(d-1)} \right)}{C_0 L_2 C_2} + \frac{d \left(\frac{V_{in}kd^2}{Ra(d-1)^2} + \frac{dV_{in}}{R(d-1)} \right)}{C_0 L_2 C_1 a} \right) + s \left(\frac{\frac{d^2 k^2 (V_{in} - \frac{V_{in}d}{d-1})}{C_0 L_2 C_1 L_1 a} - \frac{d^2 k^2 \left(\frac{(V_{in}k - \frac{V_{in}d}{d-1})}{L_1} - \frac{(1+k)V_{in}}{L_1} \right)}{C_0 L_2 C_1 a}}{\frac{d^2 ka \left(\frac{(V_{in}k - \frac{V_{in}d}{d-1})}{L_1} - \frac{(1+k)V_{in}}{L_1} \right)}{C_0 L_2 C_2} + \frac{d^2 k^2 a (V_{in} - \frac{V_{in}d}{d-1})}{C_0 L_2 C_1 L_1}}}{s^5 + \frac{s^4}{RC_0} + s^3 \left(\frac{d^2}{C_0 L_2} + \frac{-d^2}{C_1 L_2} + \frac{d^2 k^2}{C_1 L_1} + \frac{d^2 k^2 a^2}{C_2 L_1} \right) + s^2 \left(\frac{d^2}{C_1 C_0 L_2 R} - \frac{d^2}{C_2 C_0 L_2 R} + \frac{d^2 k^2}{C_1 C_0 L_1 R} + \frac{d^2 k^2 a^2}{C_1 C_0 L_1 R} \right) + s \left(\frac{d^2 k^2 a^2}{C_2 C_0 L_1 L_2} + \frac{d^2 k^2}{C_2 C_0 L_1 L_2} \right)} \quad (15)$$

By using the values given in Table 1 except snubber values that are neglected in model, the step responses of the model in (13) and (15) can be drawn with different 'd' values in Figure 7a without considering the filter effect. The figure shows the output voltage of the converter by comparing large- and small-signal models. 'd' in both models is changed as in Figure 7b.

Table 1. Parameters used in the study.

V_{in}	f	L_1	L_2	C_1	C_2	C_0	L_f	L_{f1}
100 Vrms	60 Hz	1180 μ H	654 μ H	1 μ F	1 μ F	940 μ F	35.2 mH	9.166 mH
L_{f2}	L_T	$C_{T,f}$	f_s	C_{swsnub}	R_{swsnub}	C_{dsnub}	R_{dsnub}	
10.23 mH	652 μ H	22 nF	42 kHz	1 n	150 Ω	1.8 n	150 Ω	

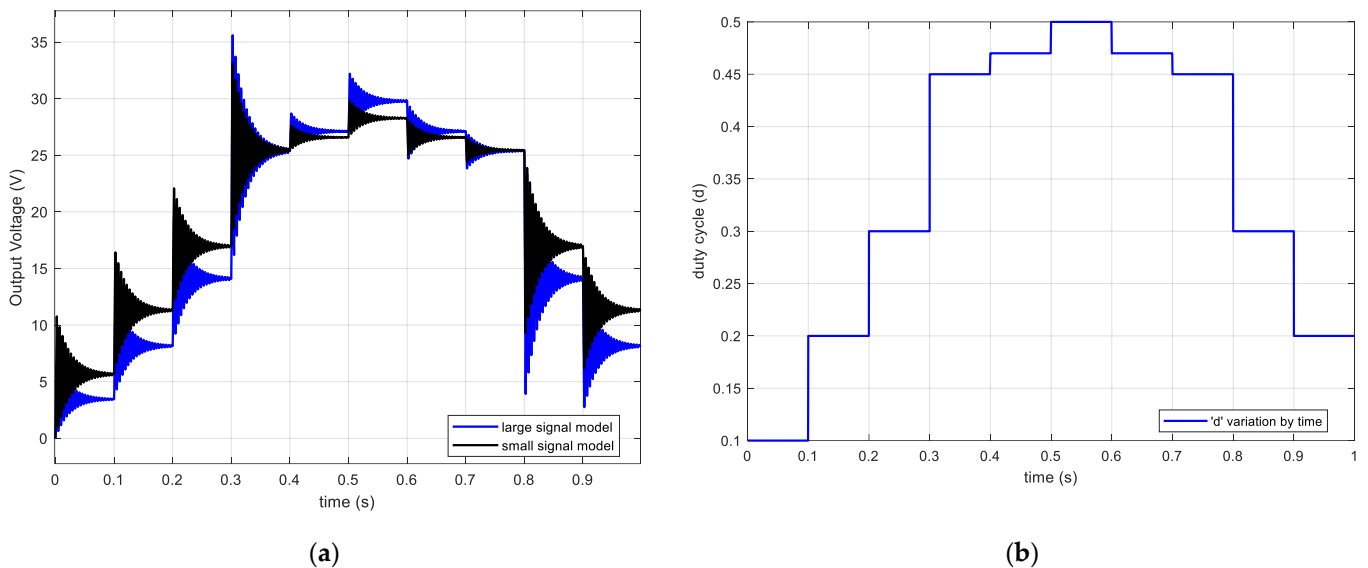


Figure 7. (a) Step responses of the large- and small-signal model regarding different d; (b) variation in d with time.

It can be seen in Figure 7 that each model is stable and their time responses are similar to each other and settle to some output voltage level. However, there is a steady-state error between the two models that becomes smaller close to the operating point.

Step responses in terms of d variation are repeated using an LCL trap filter with large- and small-signal models, and the comparison is given in Figure 8. While drawing the figure, the transfer function of the trap filter in (5) is cascaded with the large-signal model in (13) and the small-signal model in (15). It is seen in the figure that the large- and small-signal models including the filter have similar characteristics but there is a steady-state error between the two models that becomes smaller close to the operating point as seen in Figure 8. The variation in d is the same as in Figure 7b).

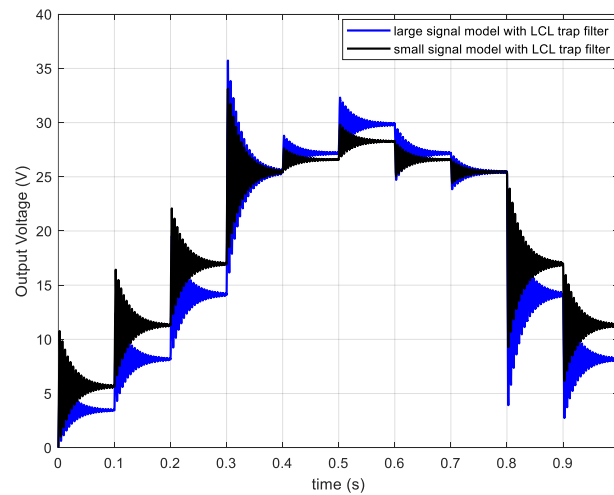


Figure 8. Step response comparison with the LCL trap filter for large- and small-signal model regarding d variation.

Bode and root locus graphs of the overall transfer function of the system consisting of the converter and filter are shown in Figure 9.

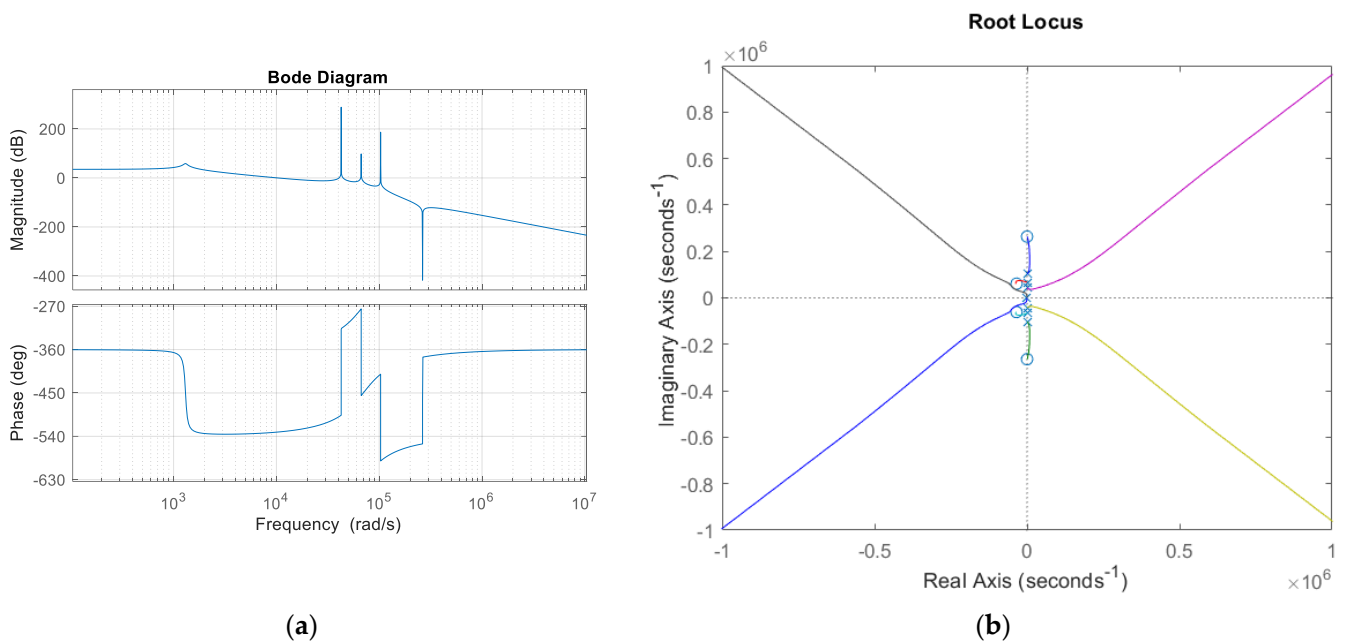


Figure 9. Overall system for the converter and the LCL trap filter (a) Bode; (b) root locus.

4. Applications

In this section, firstly, LTspice open-loop simulations for LC and LCL trap filters are conducted and measurements including the PF, THD, and output voltage are obtained. Then, the application results using the LCL trap filter are given. The application is realized by a PI controller using isolated voltage measurement. After that, the results are presented and compared. In addition, a power diode snubber is not considered in the simulations except for in the ideal case of the simulation.

The PFC isolated Ćuk converter application using the LCL trap and LC filters is conducted by laboratory set up and the LTspice simulation using the same SiC MOSFET in the application. For applications, SiC MOSFET and dsPIC30F4011 are used as shown in Figure 10. The converter is built for up to 50 W with a 42 kHz switching frequency. The measurement equipment is listed in Table 2. The values of the components used in the application are given in Table 1. Both linear and nonlinear loads are considered for both the simulation and applications. The linear load is a resistor with the value of 12.5 Ω . For the nonlinear load, six parallel 7815 voltage regulators are used. Each voltage regulator feeds a 47 Ω resistive load.

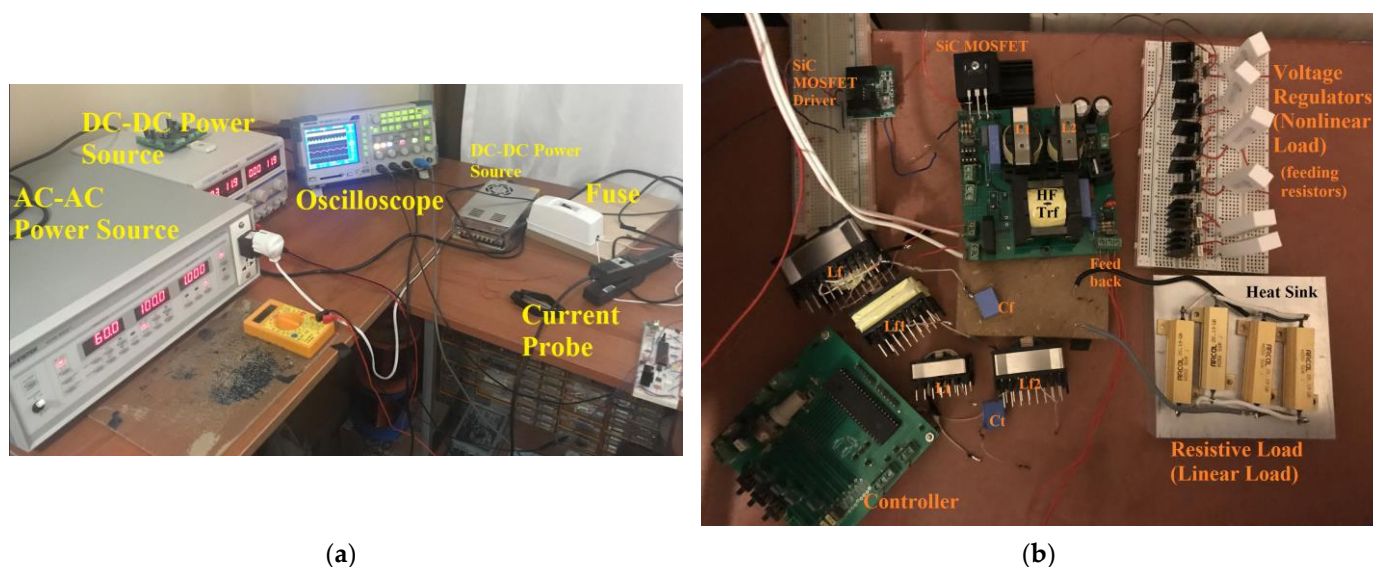


Figure 10. (a) Laboratory environment; (b) application setup.

Table 2. Equipment used for experiments.

AC Power Source	Oscilloscope	THD Measurement	Current Measurement (Probe)	Voltage Measurement (Probes)	SiC MOSFET	MOSFET Driver
GW Instek APS-9501 500VA (GOOD WILL INSTRUMENT CO., LTD., New Taipei City 236, Taiwan)	TPS2024B 4 Channel Isolated- 200 MHz (Tektronix, Beaverton, OR, USA)	TPS2PWR1 (Tektronix, Beaverton, OR, USA)	A652 (Tektronix, Beaverton, OR, USA)	P5122 HV TPP0201 LV (Tektronix, Beaverton, OR, USA)	Cree C2M0280120D (Wolfspeed, Durham, NC, USA)	CRD001 (Wolfspeed, Durham, NC, USA)

Firstly, the LTspice simulation of the system with an LC filter is conducted as shown in Figure 11 with SiC MOSFET used in the application. By means of the simulation, the output voltage, input sinusoidal voltage, and current are given.

It can be seen in Figure 12 that the input current is sinusoidal, the PF is 0.996 (0.995), and output voltage is 23.7 V.

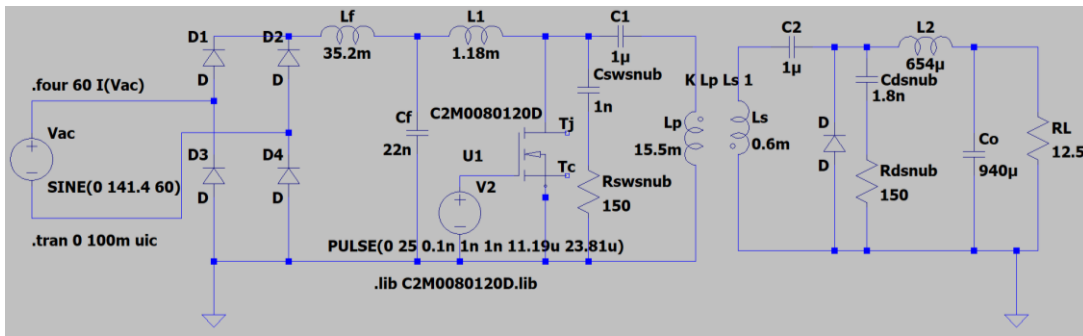
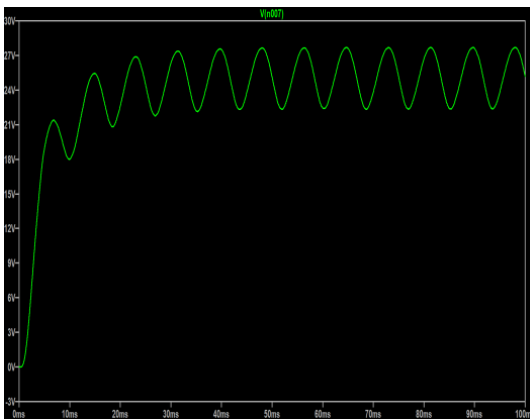
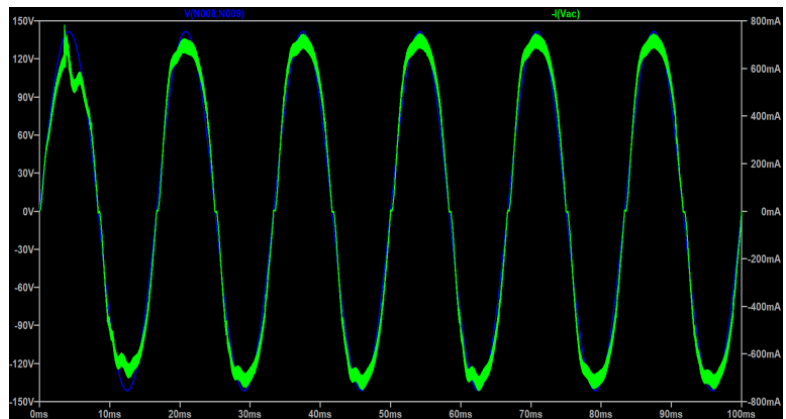


Figure 11. LTSpice simulation of the system with LC filter.



(a)



(b)

Figure 12. LTSpice with an LC filter (a) output voltage; (b) input voltage and current.

The frequency spectrum of the input current is given in Figure 13, and the THD is measured as 8.41 (9.16)%.

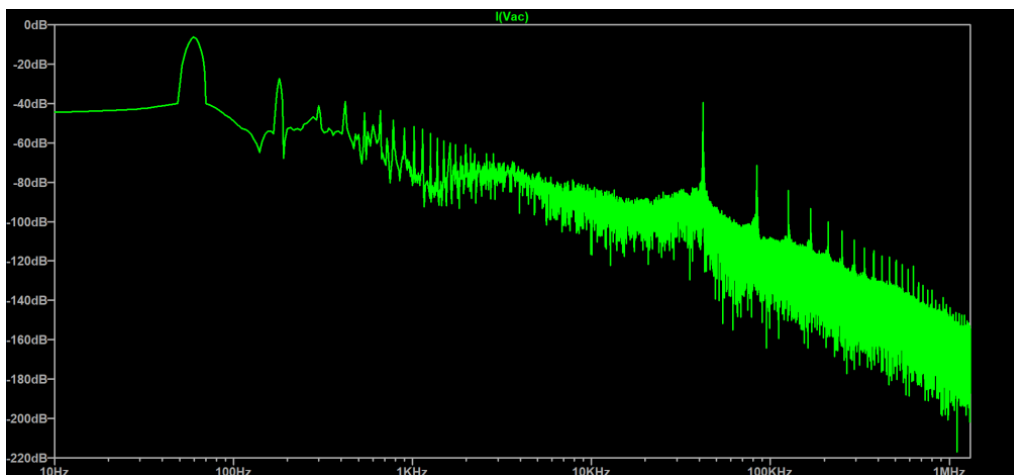


Figure 13. Frequency spectrum with an LC filter.

The LTSpice simulation of the system using an LCL trap filter with SiC MOSFET used in the application is conducted as given in Figure 14. The output voltage and input current and voltage are measured as well.

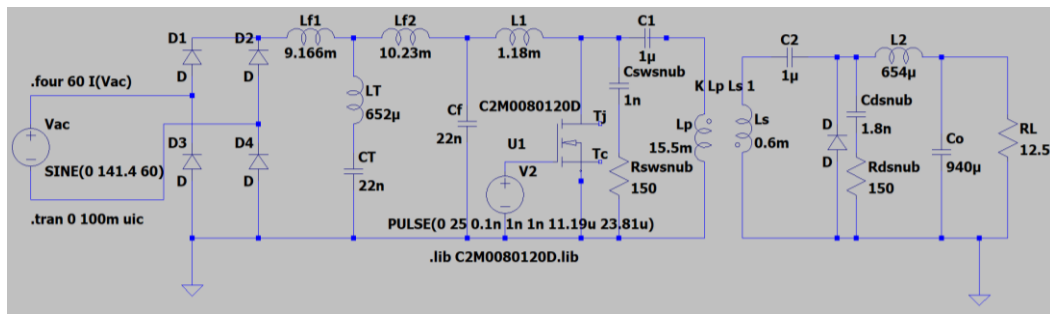


Figure 14. LTSpice simulation of the system with an LCL trap filter.

In Figure 15, the output voltage and input current and voltage are shown. It is seen that the output voltage is 24.7 V. Sinusoidal input current and voltage are obtained with a 0.997 PF.

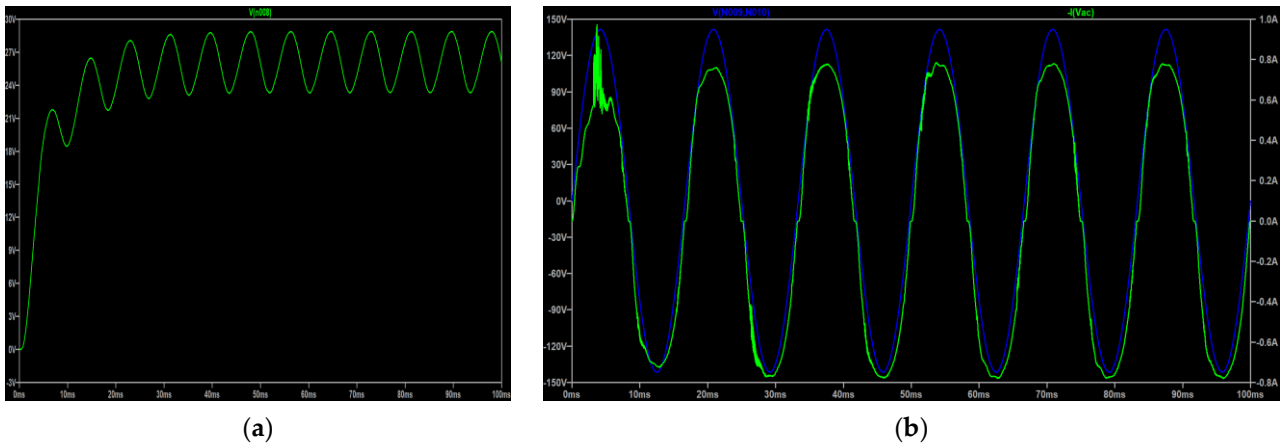


Figure 15. LTSpice with LCL trap filter (a) output voltage; (b) input voltage and current.

The frequency spectrum of the input current is given in Figure 16, and the THD is measured as 8.14 (8.41)%.

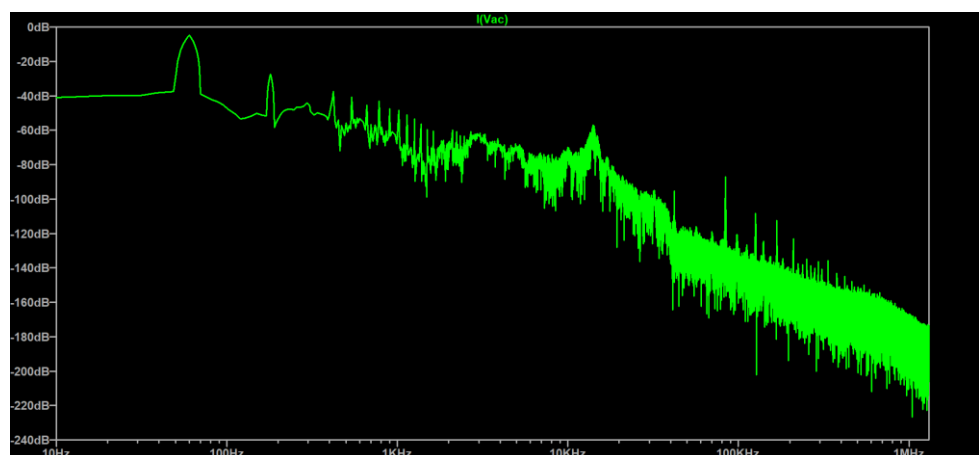


Figure 16. Frequency spectrum with an LCL trap filter.

In the simulations in Figures 11–14, the transformer is regarded as ideal and load as resistive. In addition, simulations are repeated with a nonideal transformer and nonlinear loads. The values of the transformer are listed in Table 3, and they are calculated using (16)–(20) as in [26–28]. However, the parasitic capacitances C_p , C_s , and C_{ps} are the estimated values as in [29]. Moreover, as a nonlinear load, three parallel voltage regulators feeding

resistive load are connected to the output of the PFC converter. In the equations, M is the mutual inductance, k_c is the coupling coefficient, N_1 is the primary turns number, N_2 is the secondary turns number, i_1 is the primary current, L_{lk} is the primary leakage inductance, L_m is magnetizing inductance, and L_p and L_s are the inductances of primary and secondary, respectively. R_o is the reluctance, l_c is the effective magnetic path, μ is the permeability, and A_c is the cross-sectional area of the core. An ETD34/11/17 core with N87 material is used for the transformer.

$$R_{o1} = R_{o2} = 3R_o = \frac{l_c}{\mu A_c} = \frac{78.6 \times 10^{-3}}{4 \times \pi \times 97.1 \times 10^{-6}} = 3 \times 2.9295 \times 10^5 \text{H}^{-1} \quad (16)$$

$$L_p = \frac{N_1^2}{R_{o1}} = \frac{117^2}{3 \times 2.9295 \times 10^5} = 15.5 \text{mH}, L_s = \frac{N_2^2}{R_{o2}} = \frac{23^2}{3 \times 2.9295 \times 10^5} = 0.6 \text{mH}, \quad (17)$$

$$L_m = \frac{N_1^2}{R_o} = \frac{117^2}{2.9295 \times 10^5} = 46.7 \text{mH}$$

$$M = \frac{N_1 N_2 i_1}{R_o i_1} = \frac{117 \times 23}{3 \times 2.9295 \times 10^5} = 306.195 \times 10^{-5} \text{H} \quad (18)$$

$$M = k_c \sqrt{L_p L_s} \Rightarrow k_c = 0.9877 \quad (19)$$

$$L_{lk} = L_p(1 - k_c) = 15.5 \times 10^{-3}(1 - 0.9877) = 190.65 \mu\text{H} \quad (20)$$

Table 3. Parameters of the transformer.

L_p	L_s	L_m	k_c	L_{lk}	C_p	C_s	C_{ps}
15.5 mH	0.6 mH	46.7 mH	0.9877	190.65 μH	28 pF	5.6 pF	30 pF

Using the values for the transformer given in Table 3, simulations are repeated with the model in Figure 17. Then, all the simulation results and application results are compared in Table 4.

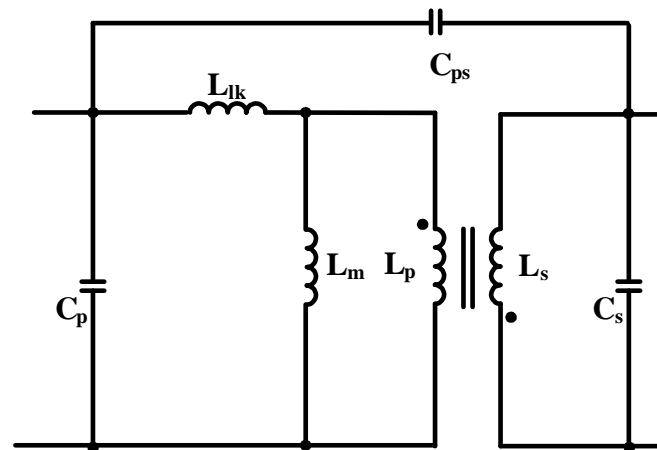


Figure 17. Exact transformer model for simulations.

The implementation results using the LCL trap filter with linear load are for output voltage and input voltage and current in Figure 18. The PF is measured as 1. Figure 18 shows the PWM signal, input voltage and current, and output voltage.

Table 4. Comparison of the simulations and applications.

	Simulation								Application			
	LC Filter				LCL Trap				Linear Load Resistive (12.5Ω)			
	PF	THD	V _o	V _{sw(m)}	PF	THD	V _o	V _{sw(m)}	PF	THD	V _o	V _{sw(m)}
Ideal (+resistive load)	0.995	9.16%	23.7 V	405 V	0.997	8.41%	24.7 V	420 V				
Resist. Load with trf. leakage	0.992	12.88%	16.54 V	1.35 kV	0.993	11.31%	17 V	1.35 kV	LCL Trap filter			
									1	4.83%	26V	600V
									LC filter			
	0.997	6.71%	24.9V [10]	520V								
Resist. Load with Cap.+ trf. leak.	0.993	11.73%	17.1 V	1.3 kV	0.992	11.87%	17.6 V	1.35 kV	Non-Linear Load (Voltage Regulator)			
Nonlinear load with trf. leak	0.992	12.07%	18.25 V	1.35 kV	0.994	10.41%	18.7 V	1.35 kV	PF	THD	V _o	V _{sw(m)}
Nonlinear load with Cap.+ trf. leak	0.995	10.43%	18.84 V	1.35 kV	0.995	10.12%	19.3 V	1.35 kV	LCL Trap filter			
									1	4.60%	26.3V	580V
									LC filter			
	0.995	6.91%	25.1V	580V								

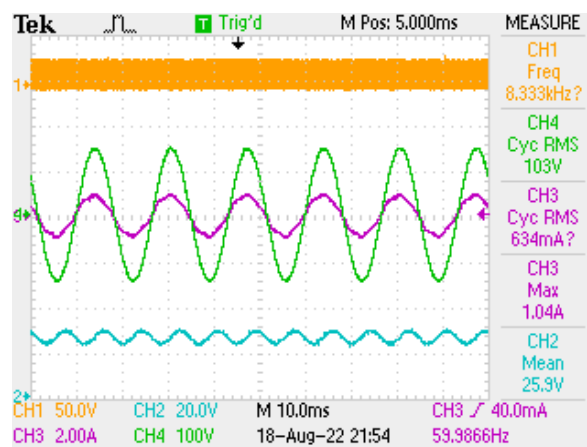


Figure 18. With LCL trap filter and linear load; PWM signal, input voltage and current, and output voltage, respectively (in the order of top to bottom).

The THD of the input current is measured as 4.83% and given in Figure 19. As the voltage THD is so low, close to 0, it is not given here.

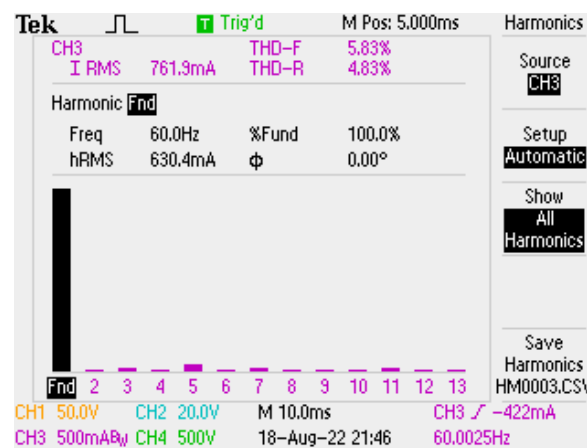


Figure 19. With LCL trap filter and linear load; input current THD.

The PF was measured with the $\cos\theta_1$ meter as 1 without considering the grid current THD. The PF is obtained as 0.998, as in (21), after considering the grid current THD.

$$PF = \frac{\cos\theta_1}{\sqrt{1 + \frac{\%THD^2}{100}}} = \frac{1}{\sqrt{1 + 0.0483^2}} = 0.998 \quad (21)$$

In addition, applications are conducted using a nonlinear load as shown in Figure 10b. The nonlinear load consists of linear regulators that have six parallel connected 7815 linear regulators and each of them is feeding a $47\ \Omega$ load. The application results using a nonlinear load are given for the LCL trap filter in Figures 20 and 21. The PF is measured as 1. The PWM signal, input voltage and current, and output voltage are given in Figure 20. The output voltage is obtained as 26.3 V.

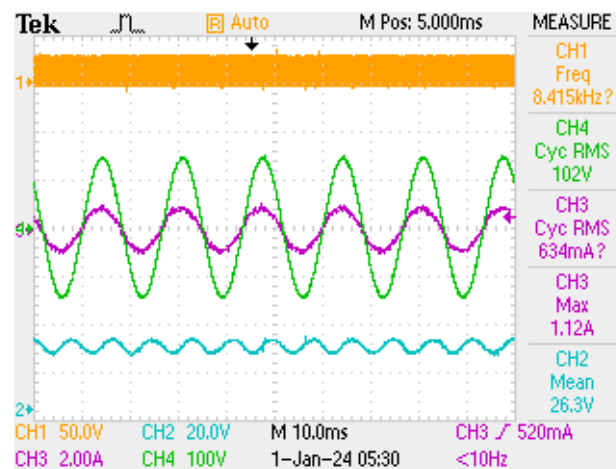


Figure 20. With LCL trap filter and nonlinear load; PWM signal, input voltage and current, and output voltage, respectively (in the order of top to bottom).

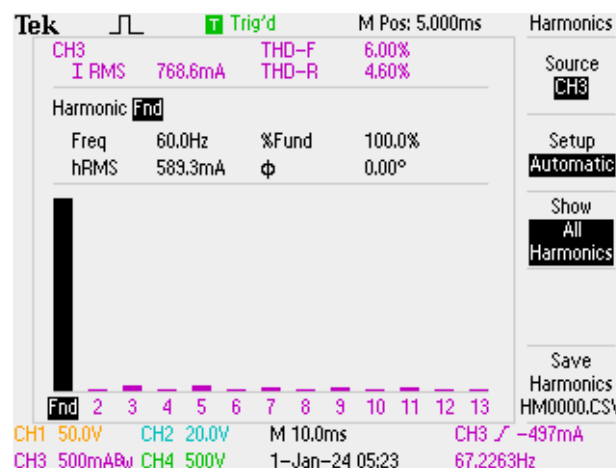


Figure 21. With LCL trap filter and nonlinear load; input current THD.

The THD of the input current of the LCL trap-filtered converter while feeding a nonlinear load is measured as 4.60% and given in Figure 21.

The LC-filtered converter was also tested using a nonlinear load and the resulting waveforms are given in Figures 22 and 23. In Figure 22, PWM signal, input voltage and current, and output voltage are given. The PF is measured as 0.995. It is seen that the output voltage is obtained as 25.1 V, though it has the same d of the LCL trap filter with a nonlinear load.

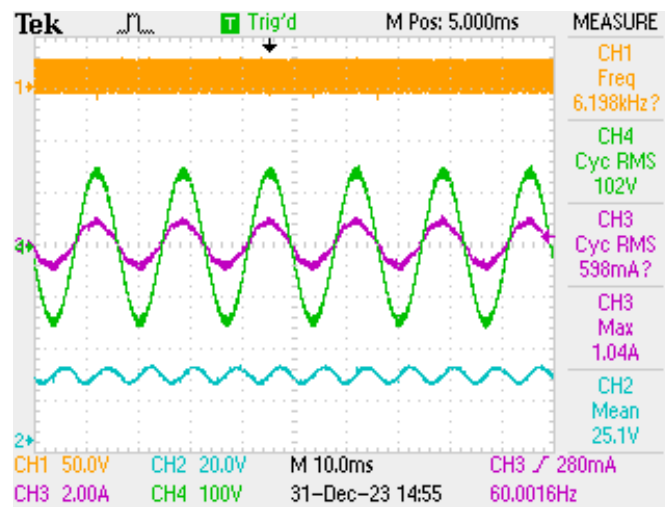


Figure 22. With LC filter and nonlinear load; PWM signal, input voltage and current, and output voltage, respectively (in the order of top to bottom).

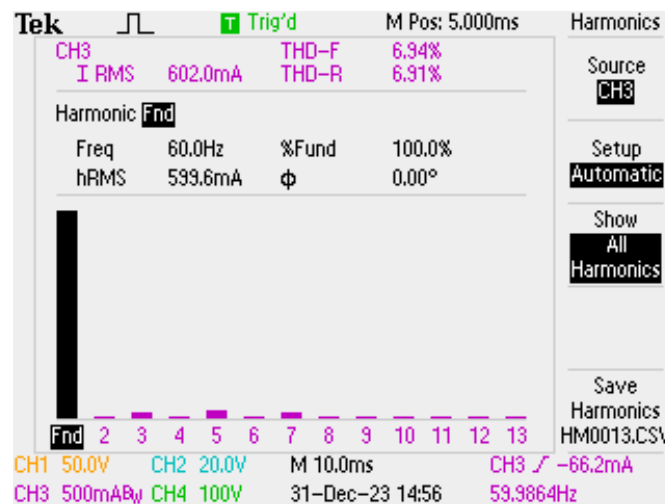


Figure 23. With LC filter and nonlinear load; input current THD.

The THD of the input current of the LC-filtered converter while feeding a nonlinear load is measured as 6.91% and given in Figure 23.

In Table 4, simulation results and application results are compared regarding the load type and transformer model used as in the ideal case, with just leakage inductance and with capacitances.

To implement closed-loop control, the output voltage as a feedback signal is measured by an isolated measurement circuit as shown in Figure 24. The isolated measurement circuit consists of a PC817 optocoupler and TL431 programmable reference IC. The circuit is shown in Figure 10b with the feedback caption. The feedback circuit reduces the cost of isolated voltage measurement compared to the sensors available commercially but the feedback voltage does not have linear characteristics.

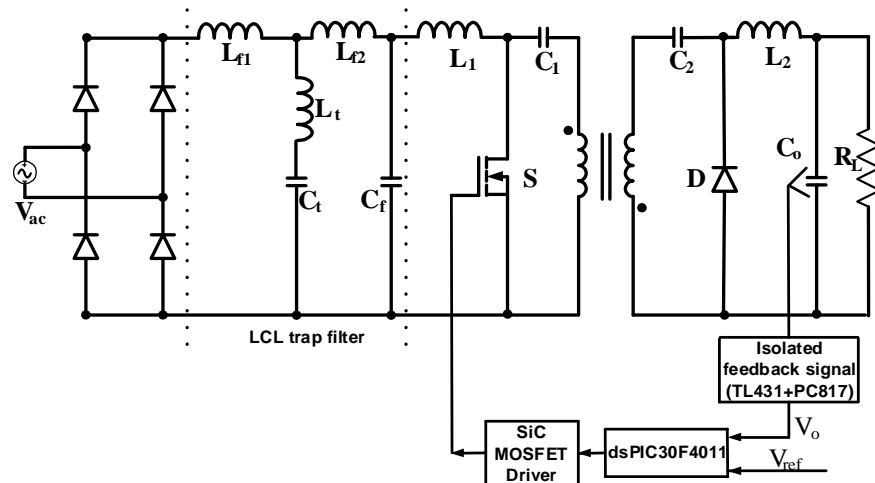


Figure 24. Closed-loop control of LCL trap-filtered isolated Ćuk PFC.

To control the output voltage, a PI controller is used. This controller can be designed using the root locus graph with the transfer function given in (22) as in [30].

$$G_{(PI)} = \frac{K_p \left(s + \frac{K_i}{K_p} \right)}{s} \tag{22}$$

The PI transfer function in (22) should be cascaded with the transfer function of the whole system including the LCL trap filter and the converter. To minimize the steady-state error, the K_p/K_i ratio should be chosen close to 0 as in [30]. After choosing the ratio as 0.001, the overall transfer function is obtained in (23).

$$T(s) = \frac{\tilde{V}_o}{d} = \frac{(1.257 \times 10^{-3}s^6 + 86.67s^5 + 9.383 \times 10^7s^4 + 6.042 \times 10^{12}s^3 + 4.302 \times 10^{17}s^2 + 4.302 \times 10^{14}s)}{(5.15 \times 10^{-20}s^{10} + 4.384 \times 10^{-18}s^9 + 8.726 \times 10^{-10}s^8 + 7.426 \times 10^{-8}s^7 + 3.869s^6 + 329.1s^5 + 4.469 \times 10^9s^4 + 3.797 \times 10^{11}s^3 + 7.607 \times 10^{15}s^2)} \tag{23}$$

By using (23), a root locus graph can be drawn as in Figure 25. The characteristics of the graph seem similar to those in Figure 9b, but it can clearly be seen that a zero is added close to the origin. According to Figure 9b, if the gain is higher than 0.0076, the system becomes unstable, so the maximum K_p should be lower than 0.0076. After choosing K_p as 0.001, K_i is obtained as 10^{-6} . For the LC filter, maximum controller gain is obtained as 3.09×10^{-4} in [10].

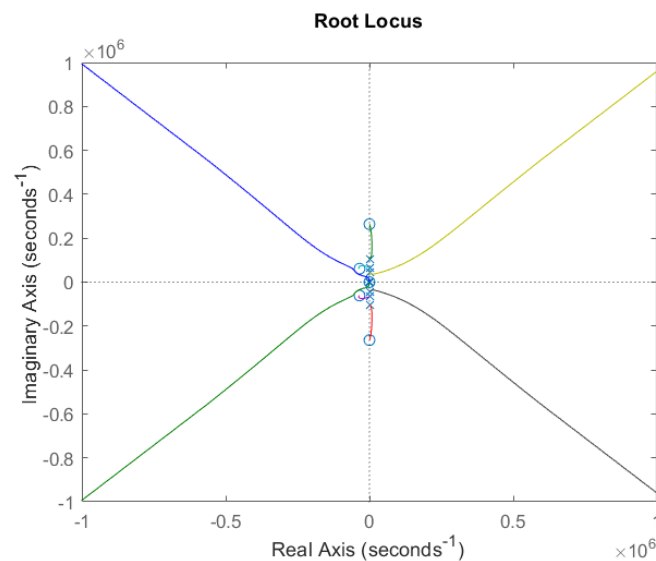


Figure 25. Root locus graph of the cascaded transfer function with $G_{(PI)}$.

With different voltage reference values, measurement is realized as shown in Figure 26. It is seen that the output voltage is regulated as desired with a maximum 1 s settling time and ± 2 V steady-state error under the reference voltage change, that is from 25 V to 10 V, from 10 V to 20 V, from 20 V to 25 V, from 25 V to 20 V, from 20 V to 10 V, and from 10 V to 25 V.

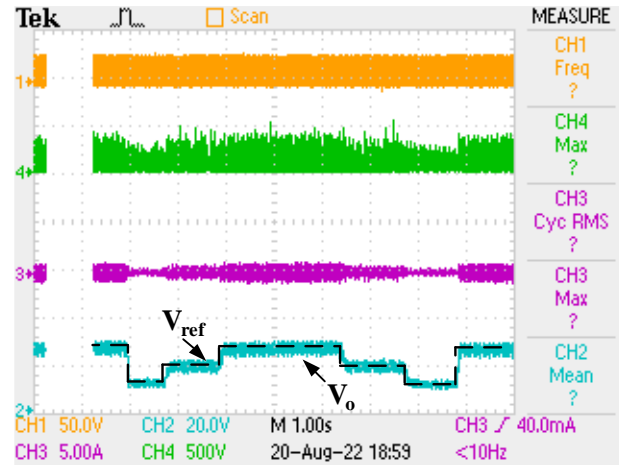


Figure 26. With LCL trap filter; PWM signal, D-S voltage of the switch, input current, and output voltage (in the order of top to bottom).

The efficiency and THD regarding the loading of the converter using LC and LCL trap filters are given in Figure 27. It is seen that the peak efficiency is 85% for the LCL trap filter and 83.4% for the LC filter. Regarding the THD of the grid current, the LCL trap filter provides 4.83% and the LC filter provides 6.71%. It is observed that the LCL trap filter ensures better results regarding THD and efficiency. Detailed analyses for the LC filter can be found in [10].

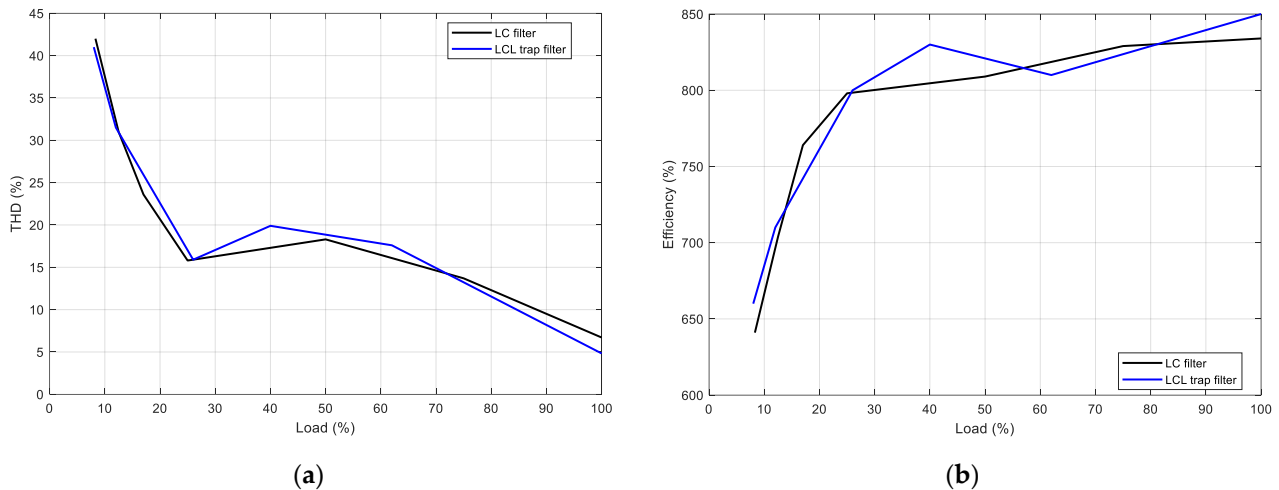


Figure 27. LC and LCL trap filter regarding load change (a) input current THD; (b) efficiency.

Efficiency (η) is determined using (24) considering the whole system. While measuring the efficiency, the input AC voltage, current, and PF are measured and the active power ($P_{ac,in}$) is calculated, the output voltage and current are measured, and the output power ($P_{dc,out}$) is calculated.

$$\eta = \frac{P_{dc,out}}{P_{ac,in}} \quad (24)$$

Further, in terms of loading, the PF comparison is given in Figure 28 for the LC and LCL trap filters. It is seen that the peak PF is obtained at full load as 0.998 as in (16) with the LCL trap filter. With the LC filter, it is obtained as 0.997.

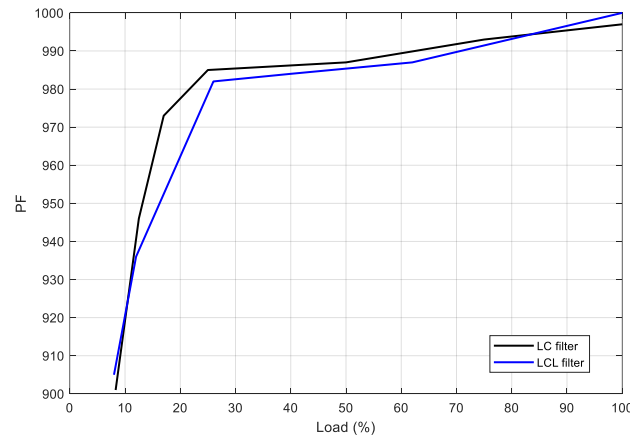


Figure 28. PF of LC and LCL trap filter regarding load change.

In addition, THDs are compared with the IEC 61000-3-2 C class standard [31] and the LCL trap and LC filters for the first 39th harmonics, and the comparison is given in Figure 29.

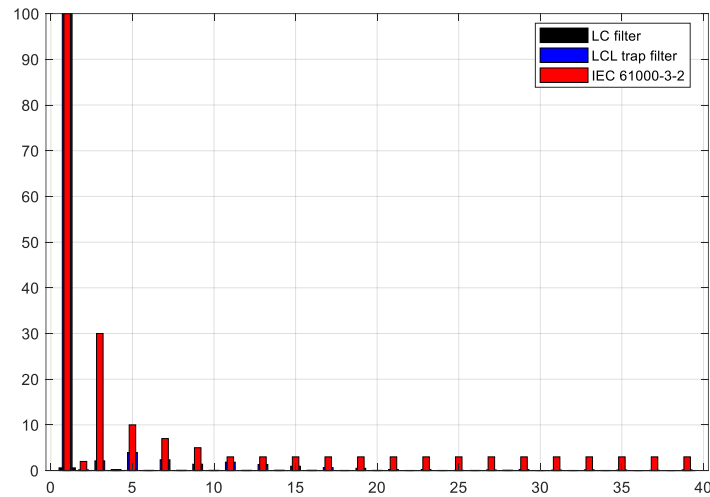


Figure 29. THD comparison of the LC, LCL trap filter, and the standard.

Loss analysis for the converter is conducted with the calculations in (25)–(46) for the LCL trap filter. The loss distribution includes DBR losses, output diode losses, copper losses, filter losses, switch losses, core losses, and output capacitor losses, with the same methodology as in [3,10,32]. Also, (25)–(41) are the same as the calculation in [10]. In the loss calculation, filter capacitance losses are neglected.

$$P_{\text{prtrf}} = I_{\text{prms}}^2 \times \text{DCR}_{\text{prm}} = 1.68^2 \times 0.4 = 1.13\text{W} \quad (25)$$

$$P_{\text{scdtrf}} = I_{\text{sdrms}}^2 \times \text{DCR}_{\text{sdr}} = 8.3^2 \times 0.01 = 0.68\text{W} \quad (26)$$

$$P_{\text{L1}} = I_{\text{L1rms}}^2 \times \text{DCR}_{\text{L1}} = 0.6^2 \times 0.5 = 0.18\text{W} \quad (27)$$

$$P_{\text{L2}} = I_{\text{L2rms}}^2 \times \text{DCR}_{\text{L2}} = 2^2 \times 0.2 = 0.8\text{W} \quad (28)$$

$$P_{\text{corepk}} = \Delta B^2 \left(\frac{f}{10^3} \right)^{1.46} \times V_e \times 10^{-6}, P_{\text{core}} = P_{\text{corepk}} \frac{2}{\pi} \quad (29)$$

$$P_{\text{coretrfpk}} = 0.4^2 \left(\frac{42000}{10^3} \right)^{1.46} \times 7630 \times 10^{-6} = 0.286\text{W}, P_{\text{coretrf}} = 0.182\text{W} \quad (30)$$

$$P_{\text{coreL2pk}} = 0.2^2 \left(\frac{42000}{10^3} \right)^{1.46} \times 5350 \times 10^{-6} = 0.050\text{W}, P_{\text{coreL2}} = 0.0319\text{W} \quad (31)$$

$$P_{\text{coreL1pk}} = 0.2^2 \left(\frac{42000}{10^3} \right)^{1.46} \times 7630 \times 10^{-6} = 0.0715\text{W}, P_{\text{coreL1}} = 0.04556\text{W} \quad (32)$$

$$P_{\text{DBR}} = 2 \times I_{\text{av}} \times V_{f,\text{brdg}} = 2 \times 0.636 \times \sqrt{2} \times 0.6 = 1.08\text{W} \quad (33)$$

$$P_{\text{swtch,cond}} = I_{\text{swrms}}^2 \times R_{\text{dson}} = 1.8^2 \times 300 \times 10^{-3} = 0.972\text{W} \quad (34)$$

$$P_{\text{swtch,snub}} = V_{\text{in}}^2 \times f \times C_{\text{snub}} = 140^2 \times 42000 \times 10^{-9} = 0.82\text{W} \quad (35)$$

$$P_{\text{diode,cond}} = I_{\text{diode}} \times V_{f,\text{diode}} = 2 \times 1.5 = 3\text{W} \quad (36)$$

$$P_{\text{diode,snub}} = V_{\text{diode}}^2 \times f \times C_{\text{snub}} = 76^2 \times 42000 \times 1.8 \times 10^{-9} = 0.436\text{W} \quad (37)$$

$$P_{\text{cap}} = I_{\text{cap}}^2 \times \text{ESR} = 1.18^2 \times 0.282 = 0.393\text{W} \quad (38)$$

$$P_{\text{Lf}} = I_{\text{Lfrms}}^2 \times \text{DCR}_{\text{Lf}} = 0.6^2 \times 1.6 = 0.576\text{W} \quad (39)$$

$$P_{\text{Lf1}} = I_{\text{Lf1rms}}^2 \times \text{DCR}_{\text{Lf1}} = 0.6^2 \times 0.3 = 0.108\text{W} \quad (40)$$

$$P_{\text{Lf2}} = I_{\text{Lf2rms}}^2 \times \text{DCR}_{\text{Lf2}} = 0.6^2 \times 0.4 = 0.144\text{W} \quad (41)$$

$$P_{\text{LT}} = I_{\text{LTrms}}^2 \times \text{DCR}_{\text{LT}} = 0.06^2 \times 0.1 = 0.00036\text{W} \quad (42)$$

$$P_{\text{coreLfpk}} = 0.2^2 \left(\frac{42000}{10^3} \right)^{1.46} \times 35600 \times 10^{-6} = 0.3338\text{W}, P_{\text{coreLf}} = 0.2126\text{W} \quad (43)$$

$$P_{\text{coreLf1pk}} = 0.2^2 \left(\frac{42000}{10^3} \right)^{1.46} \times 11500 \times 10^{-6} = 0.1078\text{W}, P_{\text{coreLf1}} = 0.0687\text{W} \quad (44)$$

$$P_{\text{coreLf2pk}} = 0.2^2 \left(\frac{42000}{10^3} \right)^{1.46} \times 11500 \times 10^{-6} = 0.1078\text{W}, P_{\text{coreLf2}} = 0.0687\text{W} \quad (45)$$

$$P_{\text{coreLTpk}} = 0.2^2 \left(\frac{42000}{10^3} \right)^{1.46} \times 3020 \times 10^{-6} = 0.0283\text{W}, P_{\text{coreLT}} = 0.018\text{W} \quad (46)$$

The loss diagram is given in Figure 30 as percentages. It is seen that higher losses of the converter are power diode losses by percentage. It is assumed that choosing a low voltage drop Schottky diode increases the efficiency by 1–2%. Further, the snubber losses of the power switches and power diode are calculated as 0.82 W and 0.436 W, respectively.

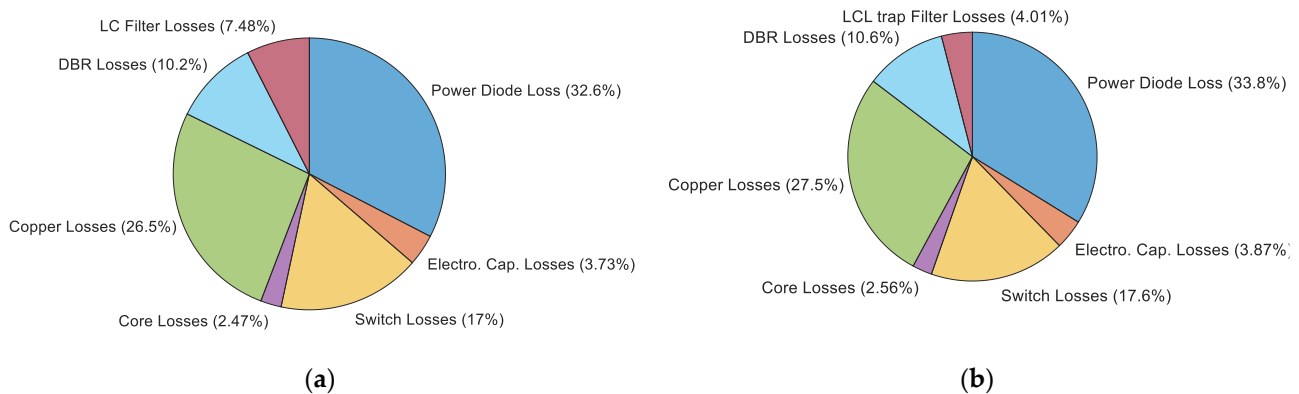


Figure 30. Loss distribution of the converter (a) LC filter; (b) LCL trap filter.

By using the loss distribution in Figure 30, the total losses are 10.5396 W for the LC filter and 10.16 W for the LCL trap filter. The output voltage of the LC filter is 25 V from [10], and from Figure 18 it is measured as 25.9 V for LCL trap filter. After taking the load as 12.5 Ω , efficiencies can be calculated as 82.5% for the LC filter and 84% for the LCL trap filter, which are close to the measured value of 85% for the operating point. An efficiency comparison of the present study with some of the studies in the literature for the same topology is given in Table 5. According to the comparison, the present study has a moderate efficiency for this 50 W power level.

Table 5. Comparison of the study with literature.

Ref.	PF	THD (%)	Eff.	Power
[3,10]	0.998–1	4.9–6.88	80–83	50 W
[33]	0.997	7.24	91.5	3.3 kW
[34]	0.97–1	3.7–7.5	70–75 for 50 W, 85 at full load	250 W
Presented	0.998	4.83	85	50 W

Filter cost is compared in Table 6. For the LC filter, an ETD54 core is used with a 35.2 mH value. On the other hand, for the LCL trap filter, two ETD39 cores and one EE25 core are used with a total value of 20.05 mH. It can be concluded that the LCL trap filter is slightly more expensive than the LC filter regarding the core and capacitance values.

Table 6. Cost comparison of the filters.

LC		LCL Trap	
Core	Capacitance	Core	Capacitance value
ETD54	1 \times 22 nF	2 \times ETD39, 1 \times EE25	2 \times 22 nF
14.86 Eur	1.63 Eur	14.44 Eur	3.26 Eur

Moreover, both filters are investigated in terms of parametric variation in the filter components, the PF and THD are measured regarding small variation in the filter parameter, and the results are given in Figure 31 after simulation for the ideal case of the transformer without considering power diode snubbers. The changes in the parameters are as follows for each filter: L_{f1} , L_{f2} , and L_f are changed by 0.1 mH; C_f and C_t are changed by 1 nF; and L_t is changed by 10 μ H. In the figure, (–) means a decrease in the parameters and (+) means an increase. In addition, initial values for the L_{f1} , L_{f2} , and L_f are taken as 9 mH, 10.2 mH and 35 mH, respectively.

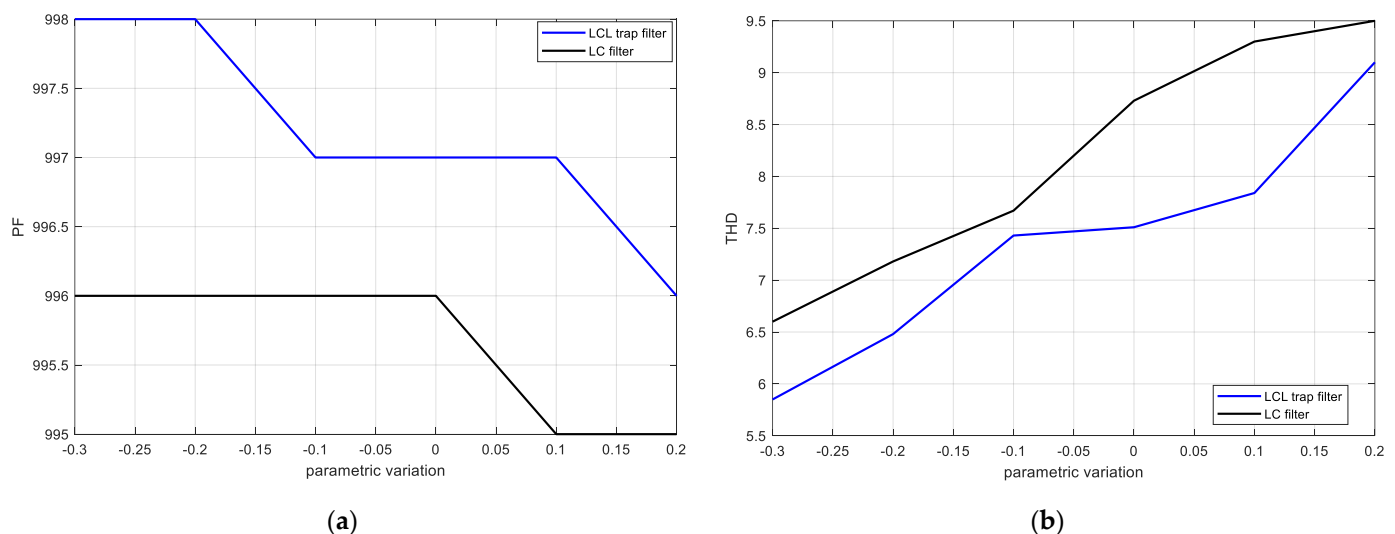


Figure 31. Parametric variation results of the filter components (a) PF; (b) THD.

It is seen in Figure 31 that when the parametric variation increases, the PF begins to decrease and THD begins to increase. However, the decreases in the PF and THD by the parametric increment

are not so drastic. On the other hand, the decreases in the PF and THD, especially the PF, are not surprising because one of the main conditions while choosing the filter in (1) is that C_f should be much lower than C_{fmax} . The increase in C_f breaks this condition, so it causes a reduction in the PF.

5. Discussion

In the present paper, a PFC isolated Ćuk converter using SiC MOSFET in DCM with an LCL trap filter is presented, which is the unique contribution of the paper because in the literature no PFC converter using an LCL trap filter has been presented.

In the simulation study, exact values of the capacitances of the transformer including interwinding and winding capacitances could not be added; instead, estimated capacitance values are used. These capacitance values affect the switch voltage stress. Furthermore, the analytical calculated values of transformer inductances, coupling coefficient, and mutual inductance are used in the simulation. To have an exact comparison for the transformer model, measured values of the implementation are better, especially for primary, secondary, and interwinding capacitances. However, the scope of this study is not to derive an exact model of the transformer. Further, simulations are repeated using a voltage regulator at the output of the converter as a nonlinear load with the exact model of SiC MOSFET in the application. The results of using a nonlinear load do not deviate much from those obtained using a linear load; the difference is maximum 0.003 for the PF and 2.9% for THD regarding both filters from Table 4. In addition, the voltage stress of the switch is higher in the simulation study except in the ideal transformer model and application results. The output voltage with the LCL trap filter is higher than that with the LC filter by up to 1 V. Moreover, the simulation study is conducted just for an open loop.

The application of the converter using LCL trap and LC filters is conducted. Modeling of the converter with an LCL trap filter in a DCM model is performed in terms of large and small signals. Further, large- and small-signal models with or without an LCL trap filter are compared using d variation, and similar results are obtained, proving that the modeling is accurate. Moreover, a large-signal model has a smaller steady-state error compared to the small-signal model. In addition, in the application, the output voltage of the converter is regulated by a PI controller designed considering the filter effect in the transfer function by the root locus method. As a result of the measurement, output voltages are regulated as desired with a maximum 1 s settling time and ± 2 V steady-state error under reference changes. Moreover, as a control characteristic for stability the LCL trap filter has a much higher gain than the LC filter. Further, the application is tested with nonlinear and linear loads separately as in the simulation; as a nonlinear load, a voltage regulator is used, and as a linear load, resistive loads are used. Regarding load type, for the LC filter the results of the THD and PF become worse with 0.002 for the PF and 0.2% for the THD under a nonlinear load compared to a linear load. For the LCL trap filter, the THD improves by 0.23% with a nonlinear load than with a linear load. However, for the nonlinear load operation, the duty cycle is increased by 0.02 to increase the output voltage compared to the linear load. However, the main results regarding the PF and THD values are slightly better in the applications than in each of the simulations.

A comparison of LCL trap and LC filters is also presented in the study for both simulation and application results. Regarding the simulations in Table 4, in each case of the simulations, the LCL trap filter gives better results for the THD and PF except for the resistive load with the model in Figure 17 with a 0.001 PF and a 0.14% THD difference. A comparison is also performed with the application for the PF and THD, and the efficiency of the LCL trap filter is higher than that of the LC filter. In addition, the efficiency value presented with the LCL trap filter is acceptable for its power rating regarding the literature presented in Table 5. A comparison with the standard is also presented and each filter meets the standards. Further, a cost comparison is presented in Table 6, and it can be concluded that the LCL trap filter is slightly more expensive than the LC filter.

Parametric variation in the filter components is considered in the study as well. As a result of the simulation regarding parametric variation, when the parametric variation has a tendency to increase in the parameters, the PF and THD begin to worsen in relation to the increment rate. On the other hand, when the parametric variation has a tendency to decrease in the parameters, the PF and THD begin to improve with the decrement rate. The result is not so surprising because of the condition of choosing the C_f . The filter capacitor should have a value much lower than the C_{fmax} .

6. Conclusions

Herein, an LCL trap filter is applied to a single-phase PFC converter, which is the main contribution of the paper. As a PFC converter, isolated Ćuk is selected with SiC MOSFET and operated with linear and nonlinear loads separately for LCL trap and LC filters. Further, large- and small-signal

models of the converter are derived and compared, which is the second main contribution of the paper. The models exhibit the same characteristics but there is a steady-state error in the large-signal model that decreases when reaching the operating point.

In addition, the filter transfer function and the design concept are introduced. A cascaded transfer function with the converter is further obtained. Large- and small-signal models using the filter effect are compared as well. Similar characteristics are obtained with the models compared to without a filter. Therefore, it can be concluded that the modeling strategy is accurate.

Moreover, LTspice simulations using SiC MOSFET for LCL trap and LC filters are conducted with an ideal transformer and exact transformer model and they support the application results. It is also concluded that the results obtained using the LCL trap filter are satisfactory and meet the existing standards and are better than the LC filter topologies regarding the PF, THD, and control characteristics. However, the cost of the LCL trap filter is slightly higher than that of the LC filter. In addition, parametric variations in the filter components are investigated, and as a result of the increase in the parameters, the PF and THD results are worsening regarding the increase rate.

Further, a controller design considering the filter behavior using the root locus method is presented for the LCL trap filter regarding the small-signal transfer function and the output voltage is regulated as desired.

Author Contributions: Conceptualization, methodology, validation, formal analysis, investigation, resources, writing—original draft preparation, writing—review and editing, supervision, and funding acquisition were realized by E.Ş. All authors have read and agreed to the published version of the manuscript.

Funding: This research was funded by Silicon Austria Labs GmbH (SAL), owned by the Republic of Austria, the Styrian Business Promotion Agency (SFG), the Federal State of Carinthia, the Upper Austrian Research (UAR), and the Austrian Association for the Electric and Electronics Industry (FEEL).

Data Availability Statement: Data are contained within the article.

Conflicts of Interest: Author Erdal Şehirli was employed by the company Silicon Austria Labs GmbH.

References

1. Middlebrook, R.D.; Cuk, S. Isolation and multiple output extensions of a new optimum topology switching DC-to-DC converter. In Proceedings of the 1978 IEEE Power Electronics Specialists Conference, Syracuse, NY, USA, 13–15 June 1978.
2. Pal, S.; Singh, B.; Shirivasta, A.; Chandra, A.; Al-Haddad, K. Improved power quality opto-couplerless Cuk converter for flickerless LED lighting. In Proceedings of the IEEE Energy Conversion Congress and Exposition (ECCE), Montreal, QC, Canada, 20–24 September 2015.
3. Sehirli, E.; Üstün, Ö. Design and implementation of high-power factor isolated Cuk converter-based LED driver with SiC MOSFET. *Electr. Eng.* **2023**, *105*, 465–476. [[CrossRef](#)]
4. Kapat, S.; Krein, P.T. A Tutorial and Review Discussion of Modulation, Control and Tuning of High-Performance DC-DC Converters Based on Small-Signal and Large-Signal Approaches. *IEEE Open J. Power Electron.* **2020**, *1*, 339–371. [[CrossRef](#)]
5. Zilio, A.; Biadene, D.; Caldognetto, T.; Mattavelli, P. Black-Box Large-Signal Average Modeling of DC-DC Converters Using NARX-ANNs. *IEEE Access* **2023**, *11*, 43257–43266. [[CrossRef](#)]
6. Khamis, A.K.; Agamy, M. Comprehensive Mapping of Continuous/Switching Circuits in CCM and DCM to Machine Learning Domain Using Homogeneous Graph Neural Networks. *IEEE Open J. Circ. Syst. Access* **2023**, *4*, 50–69. [[CrossRef](#)]
7. Huang, L. Reduced-order discrete modeling method and nonlinear analysis of a discontinuous conduction mode buck converter with a constant power load. *IEEE Open J. Circ. Syst. Energy Rep.* **2023**, *9*, 1021–1036. [[CrossRef](#)]
8. Lu, Y.; Zhong, S. Sigmoid Function Model for a PWM DC–DC Converter. *IEEE Trans. Power Electron.* **2023**, *38*, 15327–15337. [[CrossRef](#)]
9. Vaghela, M.A.; Mula, M.A. Small-signal model of two-phase interleaved coupled inductor-based high step-up gain converter in DCM. *Electr. Eng.* **2023**, *105*, 1565–1583. [[CrossRef](#)]
10. Sehirli, E. Examining the impacts of DM filters to PFC isolated Cuk converter for DCM operation by comparing Si and SiC MOSFET. *Sci. Rep.* **2023**, *13*, 4732. [[CrossRef](#)] [[PubMed](#)]
11. Vorperian, V. The effect of the magnetizing inductance on the small-signal dynamics of the isolated Cuk converter. *IEEE Trans. Aerosp. Electron. Syst.* **1996**, *32*, 967–983. [[CrossRef](#)]
12. Dai, Z.; Liu, J.; Kefeng, L.; Mai, Z.; Xue, G. Research on a Modeling and Control Strategy for Interleaved Boost Converters with Coupled Inductors. *Energies* **2023**, *16*, 3810. [[CrossRef](#)]
13. Xie, L.; Wan, D. Modeling and Harmonic Analysis of a Fractional-Order Zeta Converter. *Energies* **2023**, *16*, 3969. [[CrossRef](#)]

14. Patil, P.; Krueger, M. Modeling and Analysis of Boost Power Factor Correction Converter Operated in CrCM using Various Software Tools. In Proceedings of the PCIM Europe 2023—International Exhibition and Conference for Power Electronics, Intelligent Motion, Renewable Energy and Energy Management, Nuremberg, Germany, 9–11 May 2023.
15. Azab, M. Design approach and performance analysis of trap filter for three-phase PV grid integration systems using evolutionary search algorithms. *J. King Saud Univ. Eng. Sci.* **2021**, *33*, 491–506. [[CrossRef](#)]
16. Sehrlir, E. Analysis of LCL filter topologies for DC-DC isolated Cuk converter at CCM operation. *IEEE Access* **2022**, *10*, 113741–113755. [[CrossRef](#)]
17. Mazloum, N.; Khajehoddin, S.A. An Efficient High-power-density Integrated Trap-LCL Filter for Inverters. In Proceedings of the IEEE Applied Power Electronics Conference and Exposition (APEC), Orlando, FL, USA, 19–23 March 2023.
18. Yang, X.; Zhou, H.; Althamneh, M.; Nelms, R.M. An Evolutionary Annealing–Simplex Method for Inductance Value Selection for LCL Filters. *Energies* **2023**, *16*, 4192. [[CrossRef](#)]
19. Cantarellas, A.M.; Rakhsani, E.; Remon, D.; Rodriguez, P. Design of passive trap-LCL filters for two-level grid connected converters. In Proceedings of the 2013 15th European Conference on Power Electronics and Applications (EPE), Lille, France, 2–3 September 2013.
20. Piasecki, S.; Cantarellas, A.M.; Rabkowski, J.; Rodriguez, P. Design of AC-DC power converters with LCL + tuned trap line filter using Si IGBT and SiC MOSFET modules. In Proceedings of the IECON 2013—39th Annual Conference of the IEEE Industrial Electronics Society, Vienna, Austria, 10–13 November 2013.
21. Fang, J.; Li, X.; Yang, X.; Tang, Y. An Integrated Trap-LCL Filter With Reduced Current Harmonics for Grid-Connected Converters Under Weak Grid Conditions. *IEEE Trans. Pow. Electron.* **2017**, *32*, 8446–8457. [[CrossRef](#)]
22. Wu, W.; Zhang, Y.; Blaabjerg, F.; Chung, H.S.H. A New Type of Three-Phase Asymmetric-LCL Power Filter for Grid-Tied Voltage Source Inverter with Step-Up Transformer. *IEEE Trans. Ind. Electron.* **2022**, *69*, 11936–11945. [[CrossRef](#)]
23. Bist, V.; Singh, B. An Adjustable-Speed PFC Bridgeless Buck–Boost Converter-Fed BLDC Motor Drive. *IEEE Trans. Ind. Electron.* **2014**, *61*, 2665–2677. [[CrossRef](#)]
24. Davoudi, A.; Jatskevich, J.; Rybel, T. Numerical state-space average-value modeling of PWM DC-DC converters operating in DCM and CCM. *IEEE Trans. Power Electron.* **2006**, *1*, 1003–1012. [[CrossRef](#)]
25. Eng, V.; Bunlaksananusorn, C. Modeling of a SEPIC converter operating in Discontinuous Conduction Mode. In Proceedings of the 6th International Conference on Electrical Engineering/Electronics, Computer, Telecommunications and Information Technology, Chonburi, Thailand, 6–9 May 2009.
26. Alexander, C.K.; Sadiku, M.N.O. *Fundamental of Electric Circuits*, 4th ed.; McGraw Hill: New York, NY, USA, 2009; pp. 555–611.
27. Lecture 27 Basic Magnetic’s Issues in Transformers. Available online: <https://www.engr.colostate.edu/ECE562/98lectures/127.pdf> (accessed on 17 December 2023).
28. Hambley, A.R. *Electrical Engineering Principles and Applications*, 6th ed.; Pearson: Upper Saddle River, NJ, USA, 2013; pp. 708–743.
29. Winding Capacitance. Available online: <https://www.psm.com/sites/default/files/uploads/tech-forums-magnetics/presentations/is023-winding-capacitance.pdf> (accessed on 18 December 2023).
30. Nise, S.N. *Control Systems Engineering*, 8th ed.; Wiley: Hoboken, NJ, USA, 2019; pp. 358–419.
31. IEC 61000-3-2; Electromagnetic Compatibility (EMC)—Part 3-2: Limits—Limits for Harmonic Current Emissions (Equipment Input Current ≤ 16 A per Phase). IEC: Geneva, Switzerland, 2018. Available online: https://en.wikipedia.org/wiki/IEC_61000-3-2 (accessed on 19 November 2023).
32. PFC Boost Converter Design Guide. Available online: https://www.infineon.com/dgdl/InfineonApplicationNote_PFCCMBBoostConverterDesignGuide-AN-v02_00-EN.pdf?fileId=5546d4624a56eed8014a62c75a923b05 (accessed on 17 December 2023).
33. Rathore, N.; Gangavarapu, S.; Rathore, A.K.; Fulwani, D. Emulation of Loss Free Resistor for Single-Stage Three-Phase PFC Converter in Electric Vehicle Charging Application. *IEEE Trans. Trans. Electron.* **2020**, *6*, 334–345. [[CrossRef](#)]
34. Bist, V.; Singh, B. A Unity Power Factor Bridgeless Isolated Cuk Converter-Fed Brushless DC Motor Drive. *IEEE Trans. Ind. Electron.* **2015**, *62*, 4118–4129. [[CrossRef](#)]

Disclaimer/Publisher’s Note: The statements, opinions and data contained in all publications are solely those of the individual author(s) and contributor(s) and not of MDPI and/or the editor(s). MDPI and/or the editor(s) disclaim responsibility for any injury to people or property resulting from any ideas, methods, instructions or products referred to in the content.